



AIAA-2002-3204
WAVERIDER DESIGN METHODS FOR
NON-CONICAL SHOCK GEOMETRIES

K.D.Jones

Naval Postgraduate School
Monterey, CA

K.B.Center

Centerstage Animated Reconstructions
Lakewood, CO

**3rd Theoretical Fluid
Mechanics Meeting**
24–26 June 2002 / St. Louis, MO

WAVERIDER DESIGN METHODS FOR NON-CONICAL SHOCK GEOMETRIES

K. D. Jones[†]

Naval Postgraduate School
Monterey, California

K. B. Center[‡]

Centerstage Animated Reconstructions
Lakewood, Colorado

Abstract

A review of two methods for the design of waverider configurations with more general shock geometries is presented. In the first method the *osculating cones* approach is used to rapidly determine waveriders for constant strength shocks assuming a piecewise conical flowfield, solving the Taylor-Maccoll equation to define the post-shock flowfield. In the second method, a shock with varying curvature and strength is specified, and a cross-stream marching scheme is used to compute the post-shock flowfield by solving the Euler equations. The three-dimensional cross-stream marching problem is ill-posed, but stability is achieved through the proper choice of marching directions. Unlike most previous studies, both of these methods allow for the use of non-axisymmetric shock topologies. Several waveriders, and the flowfields about them, generated by these new methods instantaneously on desktop computers are compared to the flowfields computed using a conventional three-dimensional Euler solver, requiring the construction of a computational grid and about an hour of supercomputer time.

Nomenclature

L/D	= lift divided by drag
M_∞	= freestream Mach number
p	= pressure
U, V, W	= Contravariant velocity components
u, v, w	= Cartesian velocity components
x, y, z	= Cartesian coordinates
γ	= ratio of specific heats
θ_c	= cone angle
θ_s	= shock angle
θ_{sym}	= symmetry-plane shock angle
θ_w	= wedge angle
ρ	= density
ξ	= streamwise computational coordinate
η	= circumferential computational coordinate
ζ	= radial computational coordinate

Introduction

This paper is a review of two waverider design methods developed as thesis projects under the guidance of Professor A. Richard Seebass and his longtime colleague Helmut Sobieczky. The first, the *osculating-cones* method, treats an arbitrary constant strength shock as piecewise conical, and uses the Taylor-Maccoll equation to predict the post-shock flowfield. The second, the *cross-stream marching* method, computes the flowfield behind a general shock shape by marching the Euler equations away from the shock. The methods are described in great detail in Refs. 1 and 2, respectively, and in a more general format in Refs. 3 and 4, respectively.

During the 1980's and 1990's there was much interest in the development of high-speed aircraft, such as the National AeroSpace Plane (NASP), the High-Speed Civil Transport (HSCT) and the German Sänger, to name just a few. In the search for efficient vehicle designs, an old concept, the *waverider*, received significant attention and became the focus of many research projects, at both the university and national level.

Waveriders were first conceptualized in 1959 by Nonweiler as reentry vehicles for manned space flight.⁵ Classically defined in inviscid supersonic flow, they generated shock waves that were attached to their sharp leading edges in such a way that the vehicles appeared to ride on the shock waves, hence the name *waverider*.

Waveriders were designed using an inverse methodology, *carving* the lifting surface from a known flowfield by tracing streamlines downstream from a prescribed leading edge which lay on the shock surface. In Nonweiler's case the known flowfield was merely the two-dimensional flow over a wedge, and the leading edge was an inverted *V* or *caret*, as illustrated in Fig. 1. A freestream upper surface was assumed, providing internal volume for the configuration. The post-shock pressure acting on the lower surface was greater than the freestream pressure acting on the upper surface yielding a net lift. A similar approach was used in 1963 by Jones⁶ to generate waveriders from the flowfields about axisymmetric cones at zero incidence, as illustrated in Fig. 2.

[†] Research Associate Professor, Senior Member, AIAA

[‡] Engineering Consultant

This paper is declared a work of the U.S. Government and is not subject to copyright protection in the United States.

In the following years many researchers (Eggers *et al.*⁷ provides a nice summary) developed variations to this design approach with the primary difference being the choice of the flowfield from which the waverider was carved. In most past studies geometrically simple shock shapes such as planes or axisymmetric surfaces were chosen because exact or relatively simple approximate solutions for the post-shock flowfields were known.

Historically, waveriders were thought to be superior to other designs due to the isolation of the upper and lower surface pressures by the attached shock wave. However, if the waverider was flown at *off-design* conditions, or if viscous flow and blunt leading edges were considered, the shock would not be attached to the leading edge, and the performance should suffer. While experiments by Bauer *et al.*⁸ and McDonnell Douglas⁹ found waveriders to be competitive with other designs, they did not indicate a definitive performance advantage over other configurations.

On the other hand, waveriders, or more precisely, the inverse design techniques, offer a number of advantages for the design of high-speed aircraft. If the shock is assumed to be attached then the upper and lower surfaces may be designed independently, with the lower surface defined to generate the attached shock, and the upper surface to fulfill performance and internal volume constraints. Additionally, with some engineering knowledge, a shock and flowfield may be specified based on other design constraints, like engine size and location and inlet flow quality, and the forebody shape needed to generate the desired shock and post-shock flowfield can be inversely determined.

At that time, virtually all previous waverider design studies were limited to planar or axisymmetric flowfields; therefore, the forebody and inlet designs of full configurations were severely limited. The two methods reviewed here were developed to expand the design envelope to include much more generalized shock geometries, providing a vehicle designer with more control over the integrated vehicle design.

In the sections below, the two methods are summarized, with results from each compared to direct Euler simulations of the resultant waverider forebodies. In addition, a few examples are given of applications of the methods during the years since their original presentation.

Approach

The theory and numerical procedures used for the two methods are briefly described in the sections below. Both methods were first proposed by Sobieczky *et al.*¹⁰ with further details given in Refs. 1-4, 11-12.

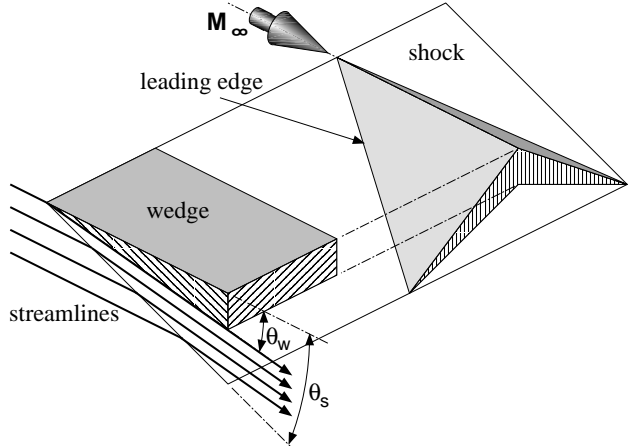


Fig. 1: Nonweiler caret-wing waverider.

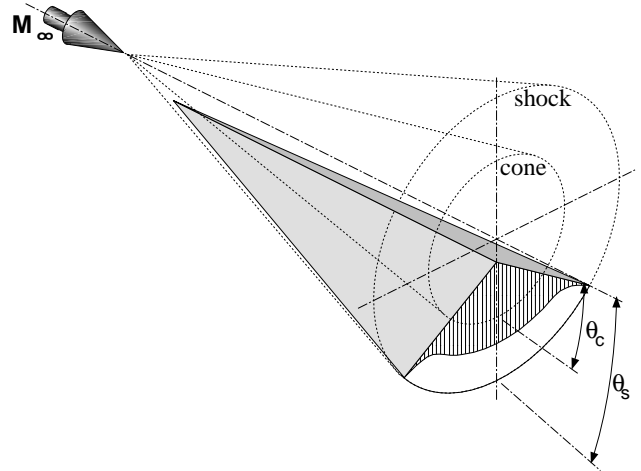


Fig. 2: Waverider derived from a conical flowfield.

Osculating Cones Method

The method of *osculating cones* is a strip-theory approach of sorts, where the flow between the shock and the lower surface is approximated by a finite number of thin strips which are aligned with the freestream flow and are locally normal to the shock surface. The flow is assumed to be conical within each of these strips. All of the strips have the same shock angle, β , and hence the same shock strength, but each strip has a local cone radius, determined by the local shock curvature. The method provides a very efficient means for generating waverider lower surfaces for a prescribed shock-shape and flow capture tube (FCT). The assumption of locally conical flow implies that the flow is everywhere tangent to these planes; hence, they can be thought of as *osculating planes* (OP). The waverider lower surface within each strip is defined by integrating a streamline downstream from the intersection of the shock surface and the FCT.

It is somewhat simpler to visualize the concept if we exclude the axial (streamwise) coordinate direc-

tion and simply look at the base plane, where the shock profile is actually defined. A waverider designed from a right circular conical shock will have local cone axes located at a common point in the plane of the configuration centerline (see Fig. 3a). If an arbitrary base-plane shock profile is specified, the local cone radii at each station along the arclength of the shock profile will have both a unique radius, due to local shock curvature, and a unique axis location, as illustrated in Fig. 3b. The dashed line in both figures is the prescribed base-plane shock profile, and the dotted lines represent the local OP, connecting the shock with the local cone center represented by the diamonds.

Lower Surface Design Generation of the lower surface of an osculating cones waverider requires the specification of a surprisingly compact set of parameters. Ambient flow conditions, namely freestream Mach number, the ratio of specific heats, and the desired shock angle, are supplemented by a user-defined base-plane shock profile and a leading edge shape to generate the lower surface of the vehicle.

The cross-sectional shape of the shock in the base plane is controlled by two analytic functions called *keys*. Each key is composed of an analytic function or a segmented combination of analytic functions that return a dependent value given a normalized input value. In the case of the lower surface, these keys define the spanwise and vertical coordinates of the shock surface at the base plane.

The resulting curve is referred to as the Inlet Capture Curve (ICC) (the solid bold line in Fig. 4a) because it can be specified as a governing geometric parameter for the generation of a waverider lower surface that produces a shock with a base-plane profile that specifically impinges upon an engine inlet lip. A third key controls the inwardly directed normal distance at each station along the ICC, defining the y , z coordinates of the FCT, which is really the streamwise projection of the leading edge. If these points are projected forward in the freestream direction, they will intersect the shock surface at some axial location, defining the x -coordinate of the leading edge within their respective conical regions, as illustrated in Fig. 4b.

The solution of the Taylor-Maccoll equation provides all flow variables as functions of a single dependent variable, the azimuthal angle. Therefore, only a single one-dimensional integration is required to define the conical flowfield. Additionally, all streamlines through the conical flow are self-similar, so only a single streamline needs to be determined, and this one streamline is then scaled appropriately in each OP to define the lower surface from the leading edge to the base plane, as illustrated in Fig. 4c.

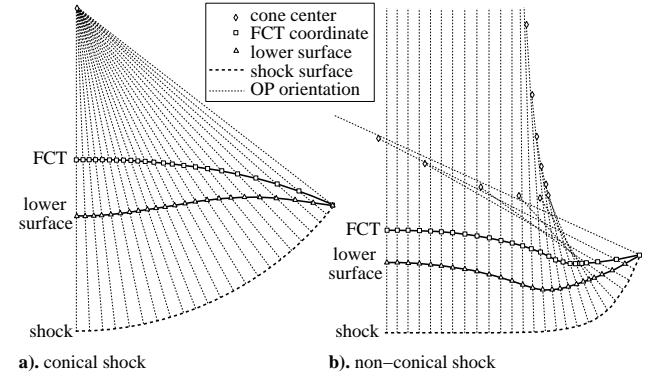
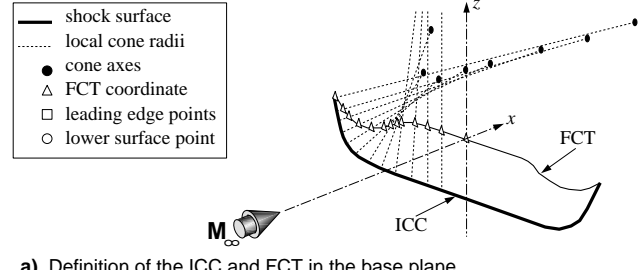
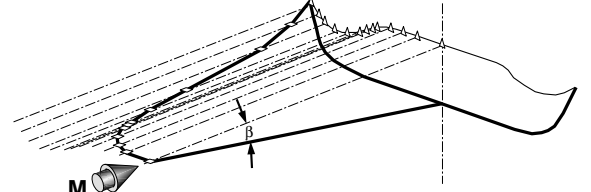


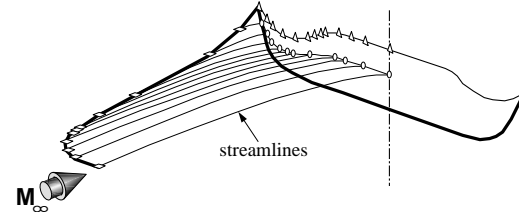
Fig. 3: Schematic for conical (a) and non-conical (b) shocks.



a). Definition of the ICC and FCT in the base plane.



b). Forward projection of the FCT to determine the leading edge points.



c). Definition of lower surface by scaled streamlines.

Fig. 4: Schematic of lower surface definition procedure.

Solution of the Taylor-Maccoll equation gives all flow variables as functions of the azimuthal angle; therefore, only this angle is needed to determine the flow properties in the region between the shock and the lower surface. Determination of the lower surface contributions to aerodynamic performance is then a simple matter of integrating these values over the lower surface computational mesh to obtain the reduced inviscid quantities of C_L , C_D and C_M .

Upper Surface Design While the lower surface geometry of the waverider is very tightly constrained by the need to maintain a continuous, attached, constant

strength shock, the upper surface leaves more to the discretion of the designer. Design of the upper surface requires consideration of two delicately balanced factors; maximum enhancement of the lift-to-drag ratio through the introduction of an expansion surface, and thoughtful allocation of the internal volume distribution to meet the packaging requirements of a practical flight application.

The shape of the upper surface is governed by two keys. The first key controls the inward deviation of the upper surface from the FCT as a function of axial location. By applying this key between the leading and trailing edges in a series of spanwise planes, the streamwise character of the upper surface can be controlled with a great deal of flexibility. In this way, complex hybrid surfaces comprised of expansion, compression, and freestream regions in any combination are easily defined. In much the same fashion, the second key is applied to scale the effect of the first key based on normalized spanwise coordinate, so that the closure of the upper surface upon the lower surface between the symmetry plane and the leading edge at the base plane can be controlled.

Determination of the primitive flow variables on the upper surface requires application of an accurate yet rapid computational analysis. This is accomplished through the application of a first-order scheme utilizing the axisymmetric method of characteristics. Once the upper surface has been defined, a family of approximate streamline-oriented marching lines must be generated to serve as the domain for application of the characteristic method. Locations are defined along the leading edge to serve as starting points. For each successive axial station, the y and z coordinates are determined by finding the intersection of the streamwise projected upper surface with the normal of the previous projection. A single marching line generated using the existing upper surface geometry can be considered to be an axisymmetric cylinder with a radius that varies as a function of streamwise coordinate, as illustrated in Fig. 5. There is one marching line for each point on the defined leading edge of the waverider.

These coordinates, along with local values of effective cylindrical radius and streamwise turning angle are computed and stored for each axial location. Flow properties along the length of each marching line are obtained through application of the compatibility equation form of the axisymmetric method of characteristics.¹³ Using freestream velocity as the starting condition, subsequent downstream primitive values are obtained by using the local values of effective radius, streamwise turning angle, and axial displacement in the compatibility equations with first-order marching techniques.

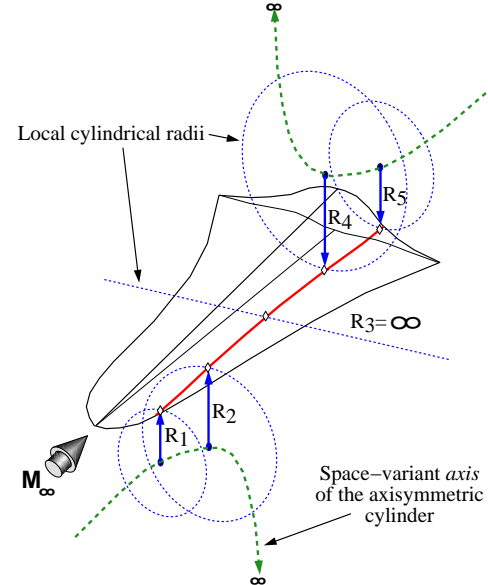


Fig. 5: Schematic of the expansion surface characteristic solver.

Once the flow variables have been obtained along all marching lines, the values are redistributed onto the original surface grid. Finally, as for the lower surface, the aerodynamic coefficient contributions from the upper surface may be calculated and combined with the lower surface values to yield the complete inviscid configuration performance values.

Viscous Effects Viscous effects play a large role in the performance of high-speed aircraft. They cause a loss in overall performance both through a substantial increase in drag coefficient and, to a lesser degree, a reduction in the lift coefficient. These losses are the result of boundary layer development along the length of the vehicle, the presence of which displaces the pressure field and leads to the addition of a skin-friction component to the drag.

The boundary layer codes applied in the analysis of both the upper and lower surfaces are derived from two-dimensional theory. Losses in accuracy from this assumption are presumed slight. Viscous effects for the waverider upper surface are computed using the streamline-oriented marching lines implemented in the upper surface pressure solution method. On the lower surface the calculations are performed along surface pseudo-streamlines within each osculating plane. Viscous analysis may only be performed after an inviscid surface solution has been obtained for the configuration and data for (p , ρ , T , M , and u) is known on the upper and lower surface pseudo-streamlines.

The analysis of the boundary layer is a three-part problem. To compute the viscous surface contribution for a full-scale aircraft, laminar, transitional, and turbulent computations must be performed to provide an

adequate representation of the boundary layer. The methods employed are from White¹⁴ as per Ref. 15. The significant difference is that the numerical approaches taken have been significantly streamlined and simplified to the point that over an order of magnitude savings in processing time is achieved.¹

If certain flight conditions are specified, the effects of viscous interaction must also be considered. In the analysis it is assumed that there is an infinitely sharp leading edge separating the flow conditions on the upper surface from those of the lower. Under realistic hypersonic flow conditions there is a significant degree of interaction between the flow near the leading edge and the boundary layer. The effect of this interaction is an induced pressure in the local freestream flow by the growth of the boundary layer in the proximity of the leading edge. This pressure increase subsequently effects the character of the boundary layer and the resulting skin friction coefficient. The majority of the effect is felt only very close to the leading edge, but the pressure increase is retained downstream. For the waveriders investigated in this study, the parameter χ , which measures the degree of viscous interaction, is much less than 1 for all locations downstream of the laminar regime. Hence the majority of viscous interaction effects are captured by applying a Reynolds analogy approximation to pressure and skin friction coefficient in the laminar regime.¹⁴

Graphical User Interface (GUI) The Waverider Interactive Parameter Adjustment Routine (WIPAR), developed by Center,¹ is an interactive design tool based on the method of osculating cones. The user functionality provided by the interface facilitates the rapid creation, modification, and optimization of waveriders in a real-time software environment. WIPAR was originally developed on the Silicon Graphics family of graphics workstations. The underlying code is written in FORTRAN and makes use of graphics library calls to provide the user interface functionality. In the years since it was originally developed, the utility has been ported to run on a variety of platforms. Even when run on platforms with limited processing resources, the efficient underlying methodology provides geometry generation and viscous surface pressure calculations on the order of seconds, providing instantaneous insight to the on-design aerodynamic characteristics of waveriders.

A screen snapshot of the WIPAR lower surface generating curve environment is shown in Fig. 6. Alterations of the flow conditions and geometric parameters that comprise the waverider are quickly made using graphical sliders, buttons, interactive graph element picking, and mouse functionality, allowing the

user to investigate the parameter space with the guidance of accumulated insight into the effects of each parameter on the performance of the vehicle.

A manual optimization procedure is available in WIPAR, where the user selects two design variables to explore, and an objective function is computed for a range of the two variables, and displayed graphically as a carpet plot. The objective function can be any one of about twenty geometric or aerodynamic values or a user defined weighted average of those values. A screen snapshot of the optimization environment is shown in Fig. 7.

The capabilities provided by the WIPAR design environment allow an investigator to develop and exercise a considerable degree of personal expertise in the waverider design process, thus introducing the element of logical human intervention. In this regard, WIPAR serves as a platform for the creation of practical waveriders that are ideally suited for specific missions.

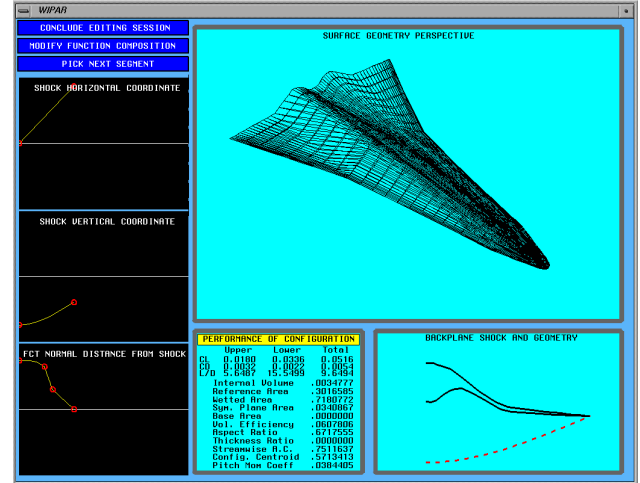


Fig. 6: Snapshot of the WIPAR lower surface generating GUI.

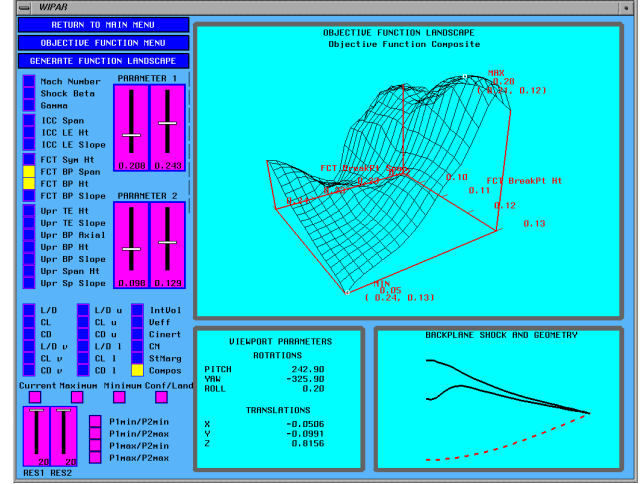


Fig. 7: Snapshot of the WIPAR performance evaluation GUI.

Cross-Stream Marching Method

The theory leading to the development of the inverse, cross-stream marching algorithm for the Euler equations was first given in Sobieczky *et al.*¹⁰ and in greater detail in Jones,² with the general methodology and a few details summarized here. The primary steps of the marching procedure are illustrated in Fig. 8. The shock geometry is first defined, and a surface mesh is generated, as shown in Fig. 8a. The post-shock flow conditions are determined using the Rankine-Hugoniot jump relations, as shown in Fig. 8b. The optimum marching directions are computed, and a new grid layer is generated, as shown in Fig. 8c. Finally, the solution is computed on the new grid layer. The last two steps are repeated iteratively to define the flow in a domain, bounded on the upstream and downstream end by characteristics, as shown in Fig. 8d. When the marching is complete, the waverider lower surface is defined by tracing streamlines through the computed flowfield, as shown in Figs. 8e and 8f. While the waverider is cut from the flowfield upstream of the base plane, the flow region downstream of the base plane is required to provide needed boundary conditions for the marching scheme. The weaker the shock strength is, the further downstream the prescribed shock must extend to provide the needed initial conditions.

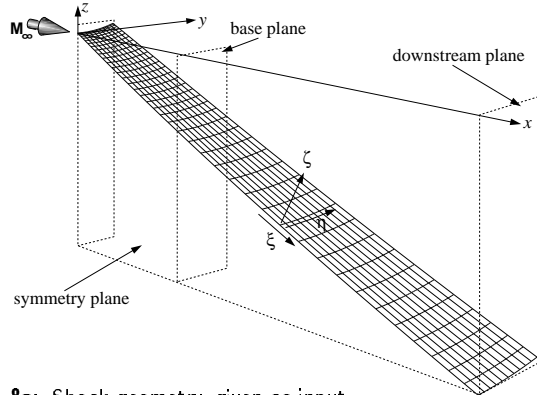


Fig. 8a: Shock geometry, given as input.

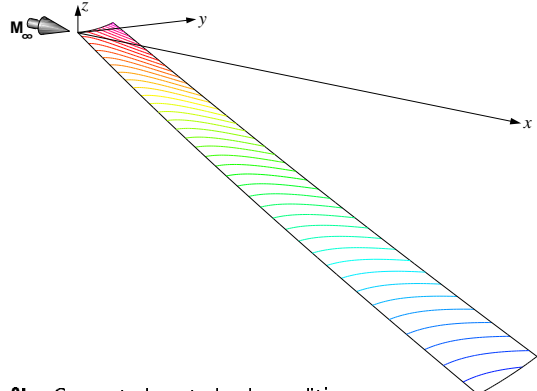


Fig. 8b: Computed post-shock conditions.

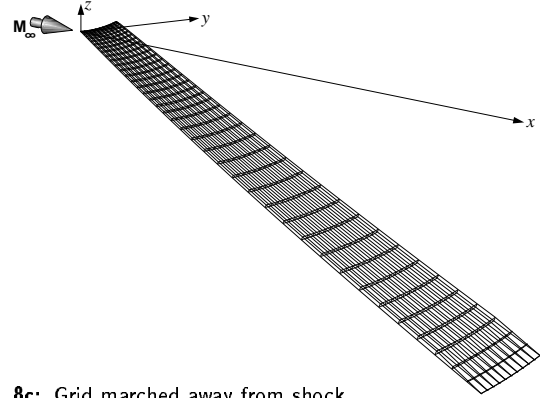


Fig. 8c: Grid marched away from shock.

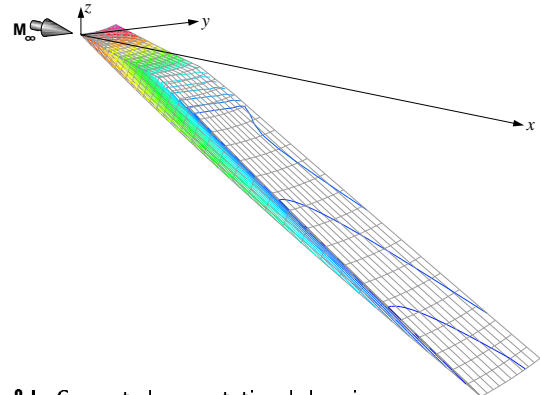


Fig. 8d: Computed computational domain.

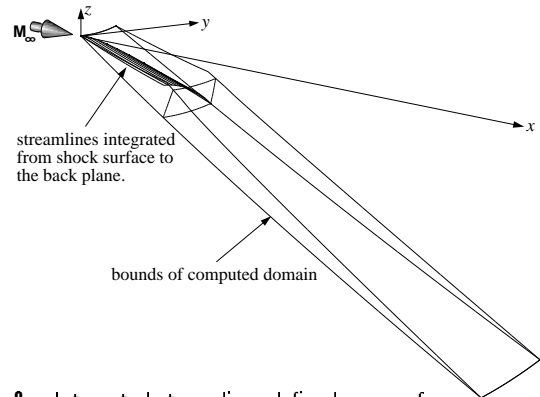


Fig. 8e: Integrated streamlines define lower surface.

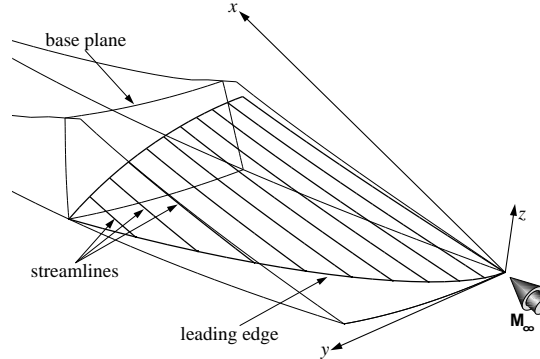


Fig. 8f: Close-up of integrated streamlines.

Posedness The virtue of such an inverse scheme is that no knowledge of a generating body is needed to define the flowfield behind a given shock. However, this is also the origin of the problem's ill-posedness.

For a mathematical problem to be well-posed, a solution must exist, be unique and be stable. While the questions of existence and uniqueness are rarely considered for problems such as this, since the governing equations are derived from fundamental laws of mechanics, the question of stability—or, more aptly, the continuous dependence of the solution on initial data—is a valid concern. In other words, do small changes in the initial data result in small changes in the solution, or do they cause large or unbounded changes in the solution?

In three-dimensional flow, the shape of the resulting shock is, in general, quite insensitive to local changes in the body's shape or, inversely, small changes in the shock shape may require large changes in the body shape or, worse yet, may preclude the existence of a solution altogether, thereby violating the stability condition for a well-posed problem. It is entirely possible to specify a shock shape for which no solution exists without the inclusion of flow features not allowed here, such as embedded shocks.

The basic principles of the ill-posedness are illustrated by considering the simple linear model equation:

$$\phi_{xx} - \phi_{yy} - \phi_{zz} = 0. \quad (1)$$

Equation (1) is a linear, hyperbolic equation in three independent variables with x as the time-like (or flow) direction. A solution can be constructed by an infinite series of modal components of the form

$$\phi = \exp[i(k_1 x + k_2 y + k_3 z)], \quad (2)$$

where $i = \sqrt{-1}$ and k_1 , k_2 , and k_3 are the wavenumbers in the respective x , y , and z coordinate directions. To march in the usual time-like direction, the wavenumber k_1 must be determined. Differentiating Eq. (2) and substituting the results into Eq. (1), one obtains

$$k_1 = \pm \sqrt{k_2^2 + k_3^2}, \quad (3)$$

such that for all real k_2 and k_3 , k_1 is real-valued, and ϕ is bounded for all x .

However, marching in a cross-stream direction implies marching in a direction different from the time-like direction—the z -direction in this case. The relation

$$k_3 = \pm \sqrt{k_1^2 - k_2^2} \quad (4)$$

is formed for k_3 as a function of k_1 and k_2 . It can be seen that for $|k_2| > |k_1|$, k_3 is imaginary valued, and

ϕ is unbounded as $z \rightarrow \infty$. Hence, this simple, three-dimensional, cross-stream marching procedure is ill-posed, that is, the solution is not continuously dependent on the initial data, unless constraints are placed on the initial data, namely, $|k_2| \leq |k_1|$.

Consider now a similar two-dimensional problem with the governing equation

$$\phi_{xx} - \phi_{zz} = 0, \quad (5)$$

with modal components of the form

$$\phi = \exp[i(k_1 x + k_3 z)]. \quad (6)$$

To march in the z -direction, the wavenumber k_3 must be determined. It is given by the relation

$$k_3 = \pm \sqrt{k_1^2}. \quad (7)$$

Hence, for all real k_1 , k_3 is real-valued, and ϕ remains bounded for all z .

In summary, the three-dimensional problem governed by Eq. (1) is only well-posed if constraints are placed on the initial data, but the two-dimensional problem governed by Eq. (5) is well-posed for all initial data. While the full system of governing equations is obviously much more complex than the simple model equations shown above, stability may still be improved by transforming the general three-dimensional system into an appropriate coordinate system where the problem is essentially two-dimensional.

Osculating Plane In a general, three-dimensional flowfield, the plane within which the flow is locally two-dimensional is called the osculating plane (OP). Both the velocity and acceleration vectors are contained in the OP, thus there is no pressure gradient normal to the OP. By transforming the system of governing equations into a curvilinear coordinate system where one family of isosurfaces is everywhere tangent to the OP, the system becomes locally a two-dimensional one in much the same way that an axisymmetric flowfield can be treated as locally two-dimensional.

Governing Equations The five equations governing the flow are the conservation of mass, the conservation of momentum, and the conservation of entropy along streamlines, given in vector notation by

$$\mathbf{E}\vec{q}_x + \mathbf{F}\vec{q}_y + \mathbf{G}\vec{q}_z = 0 \quad (8)$$

where

$$\mathbf{E} = \begin{bmatrix} u & \rho & 0 & 0 & 0 \\ 0 & \rho u & 0 & 0 & 1 \\ 0 & 0 & \rho u & 0 & 1 \\ 0 & 0 & 0 & \rho u & 1 \\ -up\gamma & 0 & 0 & 0 & \rho u \end{bmatrix}, \quad (9)$$

$$\mathbf{F} = \begin{bmatrix} v & 0 & \rho & 0 & 0 \\ 0 & \rho v & 0 & 0 & 1 \\ 0 & 0 & \rho v & 0 & 1 \\ 0 & 0 & 0 & \rho v & 1 \\ -vp\gamma & 0 & 0 & 0 & \rho v \end{bmatrix}, \quad (10)$$

$$\mathbf{G} = \begin{bmatrix} w & 0 & 0 & \rho & 0 \\ 0 & \rho w & 0 & 0 & 1 \\ 0 & 0 & \rho w & 0 & 1 \\ 0 & 0 & 0 & \rho w & 1 \\ -wp\gamma & 0 & 0 & 0 & \rho w \end{bmatrix}, \quad (11)$$

and

$$\vec{q} = [\rho \ u \ v \ w \ p]^T. \quad (12)$$

The subscripts denote partial derivatives. The use of the entropy equation in place of the energy equation is valid for the inviscid, adiabatic flows considered here. The substitution of p/ρ^γ in place of the entropy is valid for calorically perfect gases. The entropy equation is used because it lessens the coupling between the system of equations.

Equations (8-12) are nondimensionalized using $\tilde{\rho} = \rho/\rho_\infty$, $\tilde{u} = u/a_\infty$, $\tilde{v} = v/a_\infty$, $\tilde{w} = w/a_\infty$ and $\tilde{p} = p/(p_\infty \gamma)$. When these relations are substituted into Eq. (8) the system remains unchanged in form. For simplicity the tildes are dropped throughout the remainder of the development.

The equations are transformed into a generalized coordinate system where $\xi = \xi(x, y, z)$, $\eta = \eta(x, y, z)$, and $\zeta = \zeta(x, y, z)$. Expanding the partial derivatives using the chain rule, one obtains

$$\hat{\mathbf{E}}\vec{q}_\xi + \hat{\mathbf{F}}\vec{q}_\eta + \hat{\mathbf{G}}\vec{q}_\zeta = 0 \quad (13)$$

where

$$\hat{\mathbf{E}} = \begin{bmatrix} U & \rho\xi_x & \rho\xi_y & \rho\xi_z & 0 \\ 0 & \rho U & 0 & 0 & \xi_x \\ 0 & 0 & \rho U & 0 & \xi_y \\ 0 & 0 & 0 & \rho U & \xi_z \\ -Up\gamma & 0 & 0 & 0 & \rho U \end{bmatrix}, \quad (14)$$

$$\hat{\mathbf{F}} = \begin{bmatrix} V & \rho\eta_x & \rho\eta_y & \rho\eta_z & 0 \\ 0 & \rho V & 0 & 0 & \eta_x \\ 0 & 0 & \rho V & 0 & \eta_y \\ 0 & 0 & 0 & \rho V & \eta_z \\ -Vp\gamma & 0 & 0 & 0 & \rho V \end{bmatrix}, \quad (15)$$

and

$$\hat{\mathbf{G}} = \begin{bmatrix} W & \rho\zeta_x & \rho\zeta_y & \rho\zeta_z & 0 \\ 0 & \rho W & 0 & 0 & \zeta_x \\ 0 & 0 & \rho W & 0 & \zeta_y \\ 0 & 0 & 0 & \rho W & \zeta_z \\ -Wp\gamma & 0 & 0 & 0 & \rho W \end{bmatrix}. \quad (16)$$

Here U , V , and W are the contravariant velocities and ξ_x , ξ_y , ξ_z , η_x , η_y , η_z , ζ_x , ζ_y , and ζ_z are the inverse metrics.

As stated in the previous sections, marching in the OP minimizes the effects of the problem's ill-posedness. Within the OP the contravariant velocity V is by definition exactly zero. Setting $V = 0$ in Eq. (15), one obtains

$$\hat{\mathbf{E}}\vec{q}_\xi + \hat{\mathbf{F}}^*\vec{q}_\eta + \hat{\mathbf{G}}\vec{q}_\zeta = 0 \quad (17)$$

where

$$\hat{\mathbf{F}}^* = \begin{bmatrix} 0 & \rho\eta_x & \rho\eta_y & \rho\eta_z & 0 \\ 0 & 0 & 0 & 0 & \eta_x \\ 0 & 0 & 0 & 0 & \eta_y \\ 0 & 0 & 0 & 0 & \eta_z \\ 0 & 0 & 0 & 0 & 0 \end{bmatrix}. \quad (18)$$

This is the system of equations that is used to describe the flowfield between the shock and the waverider's lower surface.

Grid Generation Grid generation is an integral part of the solution procedure, as the grid must be aligned with the local osculating plane. The marching directions are determined by setting $V = 0$ and marching normal to the current ξ grid line. Marching distances are determined using a two-dimensional method of characteristics philosophy.

Marching On the shock surface and at each of the new grid planes determined by the marching procedure the partial derivatives of the primitive variables with respect to ξ and η are computed using finite differences. Remaining are five equations and five unknowns: the five partial derivatives with respect to ζ . To solve for the ζ partial derivatives, the system is inverted, yielding

$$\vec{q}_\zeta = -\hat{\mathbf{G}}^{-1}[\hat{\mathbf{E}}\vec{q}_\xi + \hat{\mathbf{F}}^*\vec{q}_\eta]. \quad (19)$$

Because of the sparseness of matrix $\hat{\mathbf{G}}$, this inversion step is easily performed. The ξ and η gradients are computed using second-order, central differences, and the solution is advanced to a new grid plane by replacing the ζ partial derivatives in Eq. (19) by second-order central differences as well.

Boundary Conditions The flowfields considered here are symmetric about $y = 0$, with the flow aligned in the positive x direction, and with the shock surface

the $\zeta = 1$ boundary. The central differenced marching step cannot be used there since no data is known at a previous step, consequently, first-order, one-sided differences are applied. Since marching is performed in the ζ direction, boundary conditions are not needed at an upper limit. The $\eta = 1$ boundary is the symmetry plane, and a second-order, central differencing, symmetry condition is applied there. The upper limit of η is handled with second-order, one-sided differences. Data here is of minimal importance, as they generally lie outside the domain of interest for the waveriders. The boundaries at $\xi = 1$ and $\xi = \xi_{max}$ are somewhat more complicated. Based on a two-dimensional method of characteristics philosophy, each new ζ grid plane is reduced by one point at each of these boundaries, so that second-order, central differences can be used to impose explicit boundary conditions without introducing instabilities to the solution. Therefore, each marched grid plane is smaller by two rows from the previous layer.

Lower Surface Definition To define the lower surface, streamlines are integrated downstream from a prescribed leading edge to the base plane. The leading edge, which lies on the shock surface, is defined by a two-dimensional arc representing either the streamwise or vertical projection, thereby defining either the FCT or the planform, respectively. The two-dimensional arc is mapped onto the shock surface using the algebraic expression defining the shock shape.

Streamline integration is performed in the computational domain for simplicity. Recall that by marching in the osculating plane, the contravariant velocity V is everywhere zero, thus the integration in computational space need only be two-dimensional. Additionally, the computational grid is uniform with unit cells, further simplifying the computation. Integration is done using the fourth-order Runge-Kutta method. The streamline coordinates in the computational domain, (ξ, η, ζ) , are then transformed into physical (Cartesian) space. All of the streamlines are combined to define the waverider's lower surface, as shown previously in Fig. 8f.

Note, while the present implementation integrates the streamlines from a prescribed leading edge downstream to the base plane, the integration could easily be reversed, integrating the streamlines forward from a prescribed lower-surface shape on the base plane to the shock surface. The intersection of the streamlines with the shock would inversely define the leading edge shape. This approach would be useful if the method were used to compute the forebody ahead of a known inlet topology.

Upper Surface Definition The upper surface geometry is up to the discretion of the designer. An option is available to generate expansion upper surfaces to enhance the overall vehicle performance. Expansion surfaces are created by first defining a freestream upper surface, and then applying a weighted average between the freestream surface and the lower surface. This averaging approach provides a flexible design method for generating open, partially closed, or closed trailing edges.

The flow parameters on the upper surface are predicted using an approximation to the axisymmetric method of characteristics. The first-order approach, developed by Center,¹ is robust, extremely fast and sufficiently accurate.

Performance Evaluation The lift and drag of the waveriders is computed by integrating the pressure forces over the surface of the waverider. The freestream pressure is subtracted from the local pressures so that pressure contributions on the upper and lower surfaces may be evaluated individually, and any contribution caused by a finite base area is removed. Nondimensional lift and drag coefficients are computed using the symmetry plane chord length as a reference length and the integrated planform area as the reference area.

Results

Extensive validation of both methods are presented in the cited references, including comparisons with theory, each other and direct numerical simulations of the resultant waverider configurations. Details of the methods used for the direct simulations can be found in Jones and Dougherty.¹⁶ The approach is briefly summarized here. Computational grids about the waveriders are formed using a transfinite interpolation grid generator. The grids are modified during the solution procedure using a spline-fitting, solution-based grid adaption scheme, and solutions are produced using the F3D Euler solver.¹⁷

Osculating Cones Method

In Fig. 9 the prescribed base-plane shock shape for five cases are compared to the pressure isolines computed by the direct solver, with the prescribed shock shown on the left, and the computed isolines shown on the right. One unavoidable consequence of the method of osculating cones approximation is that adjacent regions with different shock curvatures result in mismatched conditions that induce cross-flow velocities. The direct simulations, however, yielded no discernible displacement of the calculated shock surface from the design shock surface.

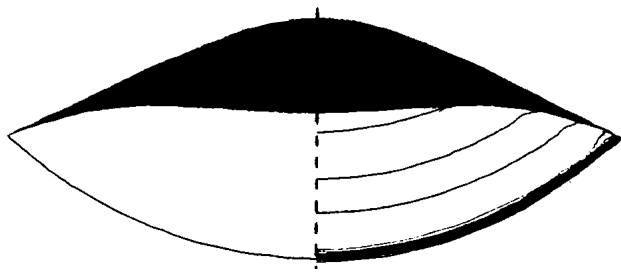


Fig. 9a: Case 1—conical shock.

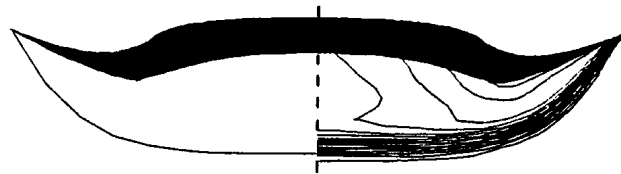


Fig. 9b: Case 2—wedge center, conical outer.

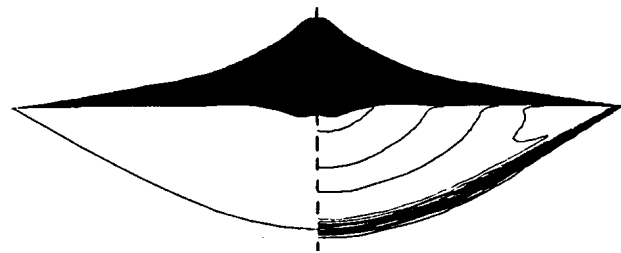


Fig. 9c: Case 3—conical inner, wedge outer.

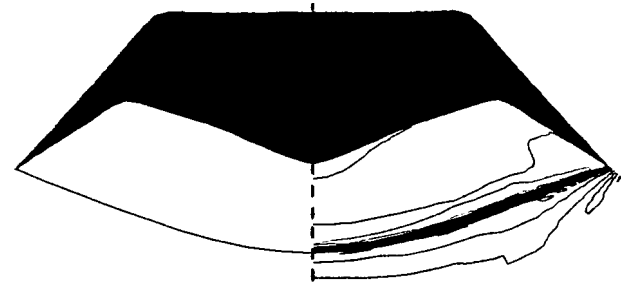


Fig. 9d: Case 4 —non-conical shock.

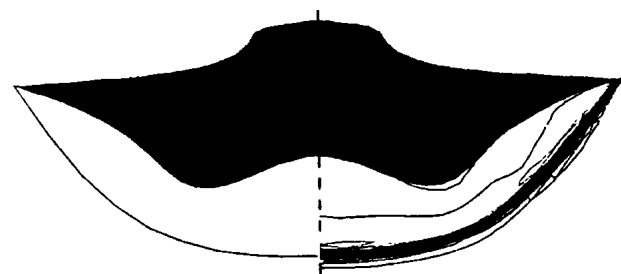


Fig. 9e: Case 5—non-conical shock.

The normalized surface pressure for the configuration shown in Fig. 10 at a cross-section 90 percent downstream from the nose and on the symmetry plane are shown in Figs. 11a and 11b, respectively, with comparisons between WIPAR and the direct solver.

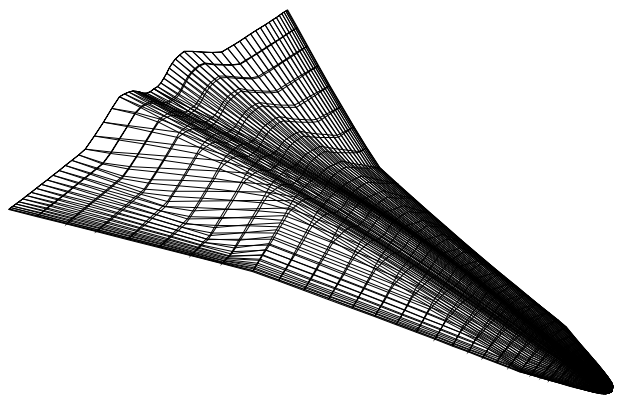


Fig. 10: Case 6—perspective view of the surface geometry.

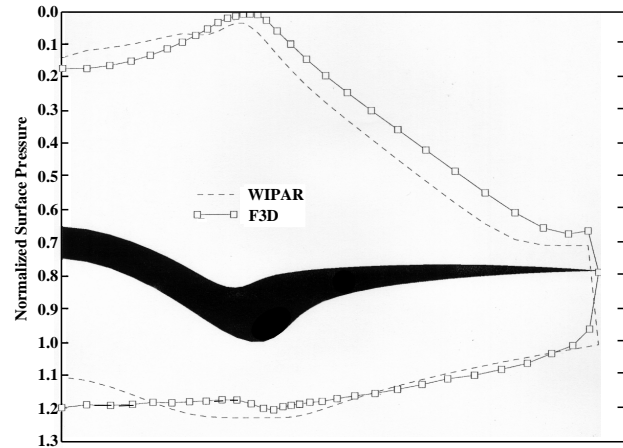


Fig. 11a: Case 6—sectional normalized surface pressure.

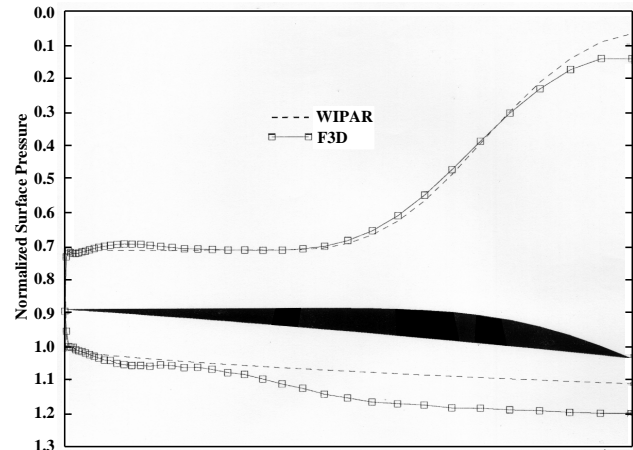


Fig. 11b: Case 6—symmetry-plane normalized surface pressure.

Pressure contours predicted by WIPAR and the direct solver are compared for two waverider topologies in Fig. 12, where the WIPAR results are shown on the right half plane of each configuration and with the F3D results on the left half plane.

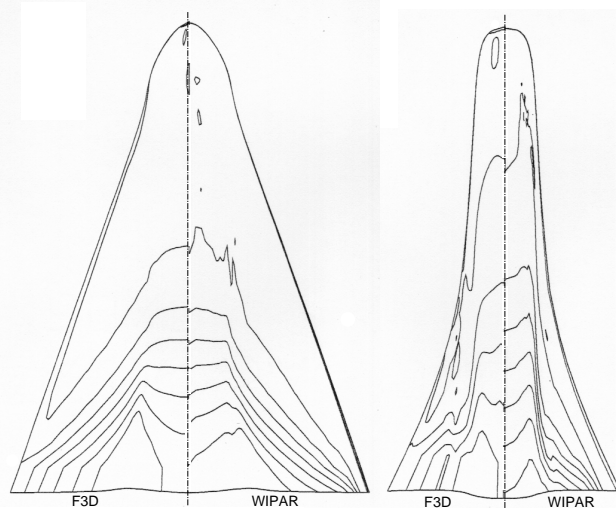


Fig. 12: Upper surface pressure contours.

Both configurations have upper surface topographies with relatively complicated combinations of spanwise curvature and axial compression/expansion characteristics. The agreement, both qualitatively and quantitatively, is impressive when it is considered that the design-process computations are made within a fraction of a second on a desktop computer.

Cross-Stream Marching Method

Validation of the cross-stream marching method, SCIMAP (Supersonic Cross-stream Inverse Euler Marching Program), can be found in Ref. 2 where comparisons with theory are used to demonstrate the accuracy of the marching scheme for simple shock geometries such as planar or axisymmetric cone shocks where solutions are compared to Rankine-Hugoniot or Taylor-Maccoll solutions, respectively. However, for most shock shapes of interest, closed-form solutions do not exist, and validation must be performed using direct simulations.

Five cases are presented here representing a range of more general shock geometries. All cases have a freestream Mach number of 4 with $\gamma = 1.4$. Computational grids for the direct simulations in all cases have $41 \times 63 \times 31$ points, and on the order of 2000 iterations are used to obtain converged solutions, with two intermediate grid refinement steps.

Sensitivity of the marching code to M_∞ and shock angle is discussed in Ref. 2. In short, the marching scheme does not have stability limits with reference to either, but grid generation becomes more difficult as the shock strength becomes small due to the increasing downstream length of the required initial data. These five cases have sufficiently strong shocks such that grid generation is not a problem.

The first two cases have shocks cut from elliptic cones with elliptic axis ratios of $a/b = 0.75$ and $a/b = 1.25$, respectively, where a is the spanwise elliptic axis, and b is the vertical elliptic axis. Both have a symmetry plane shock angle of 26.6° and freestream upper surfaces, so the pressure on the upper surfaces should be $1/\gamma$. The computed surface topologies and sectional surface pressure distributions for cases 1 and 2 are shown in Figs. 13 and 14, respectively. Agreement with the direct solver is outstanding, with only minor differences at the leading edge where the direct solver tends to smear the shock over several grid cells.

Case 3 has a shock cut from an axisymmetric cone with a 20.9° half-angle. The conical shock is canted up at a 5.7° angle such that the symmetry-plane shock angle is again 26.6° , and the upper surface has a slight expansion, so the upper surface pressure should be lower than freestream. The surface topology and sectional surface pressure distribution for case 3 are shown in Fig. 15, and both the upper and lower surface pressure agree well with the direct solver.

The shock in case 4 is cut from an axisymmetric surface with the shock angle varying from 27.7° at the nose, to 25.6° at the base plane, to 20.3° at the downstream plane. A variable expansion is used on the upper surface with a closed trailing edge on the outer portion of the body. The topology and surface pressure distribution for case 4 are shown in Fig. 16. The lower surface pressure agrees well with the direct solver, but the inflection-point on the expansion upper surface appears to be problematic for the pressure prediction there.

Case 5 has a more general shock shape. The shock is cut from a conoid with the same symmetry-plane profile as case 4 but with elliptic cross-sections with $a/b = 0.65$. This waverider also has an expansion upper surface. The surface topology and sectional surface pressure distribution for case 5 are shown in Fig. 17, and the agreement with the direct solver in this case is excellent.

Integrated lift and drag coefficients for the five cases are presented in Table 1. Agreement is quite good in all cases. The expansion upper surfaces in cases 3, 4, and 5 account for 4.5%, 15%, and 6.2% of the net lift coefficients, respectively.

Although the streamwise shock curvature in cases 4 and 5 is quite small, the effect on the flowfield is substantial, as can be seen in Fig. 18. The pressure isolines in Fig. 18a, for the constant-strength shock at the symmetry plane, are clearly linear, resulting in a pressure gradient between the shock and the waverider surface that is essentially constant for all streamwise locations.

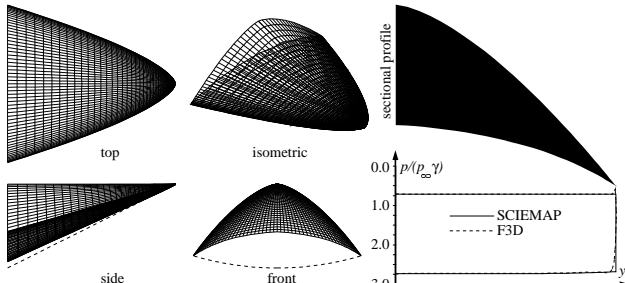


Fig. 13: Case 1—elliptic-cone shock with $a/b=0.75$ ($\theta_{sym}=26.6^\circ$).

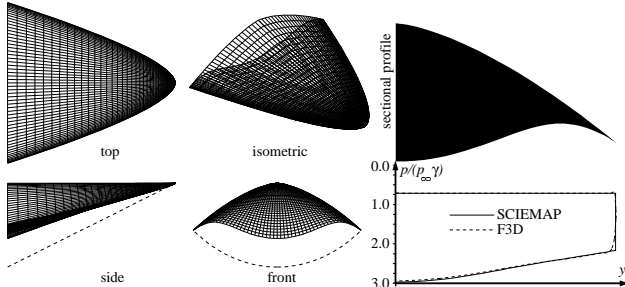


Fig. 14: Case 2—elliptic-cone shock with $a/b=1.25$ ($\theta_{sym}=26.6^\circ$).

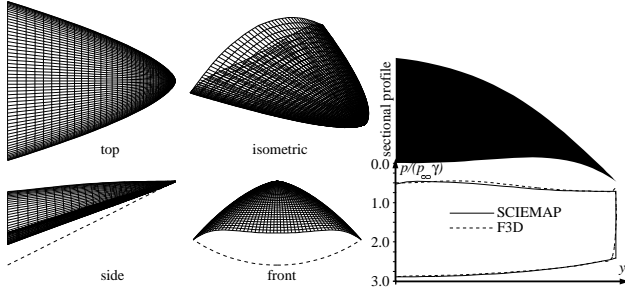


Fig. 15: Case 3—axisymmetric-cone shock at an angle ($\theta_{sym}=26.6^\circ$).

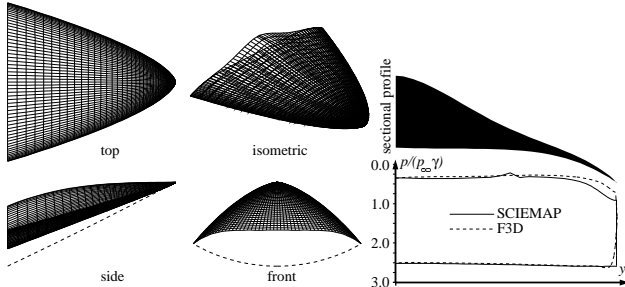


Fig. 16: Case 4—axisymmetric, variable strength shock.

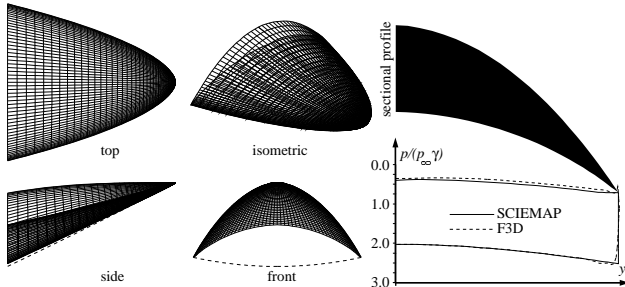


Fig. 17: Case 5—non-axisymmetric, variable strength shock.

Table 1: Comparison of lift and drag

case	code	C_L	C_D
1	SCIEMAP	0.2469	0.06609
	F3D	0.2444	0.06536
2	SCIEMAP	0.2403	0.06782
	F3D	0.2366	0.06669
3	SCIEMAP	0.2615	0.06948
	F3D	0.2605	0.06862
4	SCIEMAP	0.2630	0.06590
	F3D	0.2650	0.06590
5	SCIEMAP	0.2249	0.05246
	F3D	0.2263	0.05218

The pressure isolines in Fig. 18b, for the variable-strength shock at the symmetry plane, are far from linear, and in this case the pressure gradient between the shock and the surface varies with the streamwise location. Therefore, with a little engineering intuition, it would be possible to tailor the shock curvature in such a way as to prescribe a desired pressure gradient at some downstream location where, for example, the inlets may reside.

The marching grids in all 5 cases have 41 points in the streamwise and spanwise directions, and 12, 15, 16, 17, and 20 points in the marching direction, respectively. Computations are run on a desktop computer and require a fraction of a second to complete.

Application of the Methods

The *osculating-cones* waverider design method has been used in a number of studies in the years following its first publication, at the University of Colorado, at other universities, and in adjunct research at the DLR Institute of Aerodynamics in Braunschweig, Germany, as outlined below.

In 1993, Eggers *et al.*¹⁸ used WIPAR as a design tool to quantify the effects of various flowfield and geometric dependent parameters on the aerodynamic and stability characteristics of mission-oriented waveriders. The parameters investigated consisted of shock angle, wing camber and wing aspect ratio. The investigative research yielded several new waveriders that exhibited favorable performance characteristics compared to more conventional configurations.

In a 1996 study by Takashima and Lewis at the University of Maryland,¹⁹ the airframe/engine-integration and volumetric-distribution advantages offered by the osculating-cones approach were noted, and they produced several configurations with roughly planar shocks in front of the engines, and roughly conical flow in the outer span, following the lead of early osculating-cones waveriders generated by Sobieczky *et al.*¹⁰

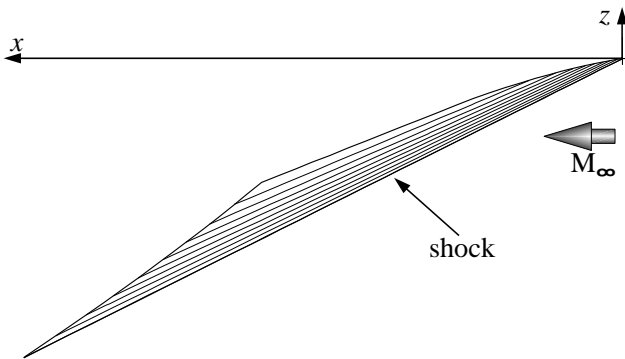


Fig. 18a: Symmetry-plane pressure isolines for case 2.

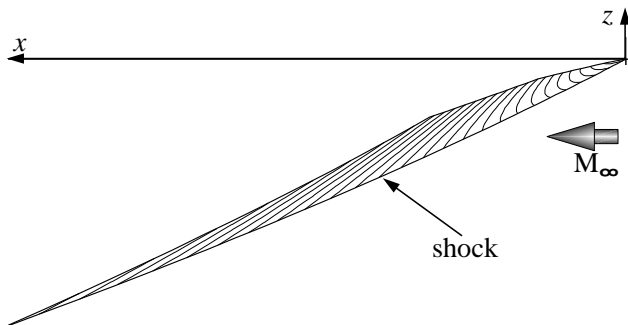


Fig. 18b: Symmetry-plane pressure isolines for case 5.

In support of arguments made in the introduction of this paper, in their conclusions, Takashima and Lewis¹⁹ suggested that the wave-riding surfaces are probably best suited as integrated components of a complete vehicle, rather than as vehicles themselves. In particular as forebody surfaces upstream of the engines, providing a means of tailoring the flow properties ahead of the inlet. This supports the concept that the waverider itself is not the end goal, but rather the inverse design procedure.

In a 1998 study by Miller *et al.*,²⁰ aluminum models of Mach 4 and Mach 6 WIPAR-generated waveriders with identical planform geometries were tested in the Langley Research Center Unitary Plan Wind Tunnel and 20 inch Mach 6 Blowdown Tunnel, respectively. The goal was to validate the osculating cones approximations by careful measurement of the aerodynamic characteristics of the two viscous optimized waveriders using force balance techniques, surface pressure measurement, and vapor screen visualization. The study was able to confirm shock placement in the on-design test runs, as well as reasonable agreement of surface pressure values within measurement limitations. The force balance measurements yielded valuable information as to the off-design characteristics of the waveriders and verified the viscous on-design aerodynamic coefficients calculated in the design process to within 5 percent.

The WIPAR-generated Mach 4 waverider investigated in the experimental study by Miller *et al.*²⁰ was also included in a high altitude aerodynamic performance study by Graves and Argrow²¹ in 2001. A Monte Carlo impact method was employed to investigate both on and off-design aerodynamic performance characteristics of the WIPAR-generated waverider, a caret-wing, and a delta-wing. The three configurations were chosen such that length, span and volume were matched. Results of the simulations showed that the osculating cones waverider and caret-wing configuration performed better than the conventional delta-wing at low angles of attack and on-design Mach number. Additionally, the WIPAR-derived vehicle provided better *L/D* performance than both of the other configurations at low angles of attack above altitudes of 120 km due to the compression surface concavity.

As far as the authors are aware, use of the cross-stream marching method has not been reported in the literature since its release in 1993.

Acknowledgments

This paper is given in memory of our advisor and mentor, Professor A. Richard Seebass. Additional thanks go to Helmut Sobieczky for his guidance and intellectual contributions to both projects.

References

- ¹ Center, K. B., "An Interactive Approach to the Design and Optimization of Practical Hypersonic Waveriders," Ph.D. Dissertation, Department of Aerospace Engineering Sciences, University of Colorado, Aug. 1993.
- ² Jones, K. D., "A New Inverse Method for Generating High-Speed Aerodynamic Flows With Application to Waverider Design," Ph.D. Dissertation, Department of Aerospace Engineering Sciences, University of Colorado, May 1993.
- ³ Center, K. B., Sobieczky, H. and Dougherty, F. C., "Interactive Design of Hypersonic Waverider Geometries," AIAA Paper No. 91-1697, June 1991.
- ⁴ Jones, K. D., Sobieczky, H., Seebass, A. R. and Dougherty, F. C., "Waverider Design for Generalized Shock Geometries," **Journal of Spacecraft and Rockets**, Vol. 32, No. 6, Nov.-Dec. 1995, pp. 957-963.
- ⁵ Nonweiler, T. R. F., "Aerodynamic Problems of Manned Space Vehicles," **Journal of the Royal Aeronautical Society**, Vol. 63, 1959, pp. 521-528.
- ⁶ Jones, J. G., "A Method for Designing Lifting Configurations for High Supersonic Speeds Using the Flow Fields of Non-Lifting Cones," Royal Aircraft Establishment, Report No. Aero. 2674, March 1963.

- ⁷ Eggers, A. J. Jr., Ashley, H., Springer, G. S., Bowles, J. V., and Ardema, M. D., "Hypersonic Waverider Configurations From the 1950's to the 1990's," Proceedings of the *1st International Hypersonic Waverider Symposium*, Oct. 17-19, 1990.
- ⁸ Bauer, S. X. S., Covell, P. F., Forrest, D. K. and McGrath, B. E., "Preliminary Assessment of a Mach 4 and a Mach 6 Waverider," Proceedings of the *1st International Hypersonic Waverider Symposium*, Oct. 17-19, 1990.
- ⁹ Kandebo, S. W., "Waverider Tests Boost Credibility," *Aviation Week & Space Technology*, Vol. 139, No. 11, Sept. 13, 1993, pp. 61-63.
- ¹⁰ Sobieczky, H., Dougherty, F. C. and Jones, K. D., "Hypersonic Waverider Design from Given Shock Waves," Proceedings of the *1st International Hypersonic Waverider Symposium*, Oct. 17-19, 1990.
- ¹¹ Sobieczky, H., Dougherty, F. C., Jones, K. D., Center, K. B. and Seebass, A. R., "Analysis of Hypersonic Waverider Forebodies With Inlets," Proceedings of the *International Aerospace Congress 1991*, Melbourne Australia, May 1991, pp. 402-417.
- ¹² Center, K. B., Jones, K. D., Dougherty, F. C., Seebass, A. R., and Sobieczky, H., "Interactive Hypersonic Waverider Design and Optimization," Paper No. ICAS-92-1.8.3, Proceedings of the *18th Congress of ICAS*, Beijing, People's Republic of China, Sept. 1992, pp. 1571-1580.
- ¹³ Ferri, A., Theory of High-Speed Aerodynamics, Princeton Series, Sears, W. R., (Editor), Vol. 6, 1954, pp. 616-623.
- ¹⁴ White, F. M., Viscous Fluid Flow, McGraw-Hill, New York, 1974, pp. 653-657.
- ¹⁵ Bowcutt, K. G., "Optimization of Hypersonic Waveriders Derived from Cone Flows - Including Viscous Effects," Ph.D. Dissertation, Department of Aerospace Engineering, University of Maryland, 1986.
- ¹⁶ Jones, K. D. and Dougherty, F. C., "Numerical Simulation of High-Speed Flows About Waveriders with Sharp Leading Edges," **Journal of Spacecraft and Rockets**, Vol. 29, No. 5, Sept.-Oct. 1992, pp. 661-667.
- ¹⁷ Ying, S. X., Steger, J. L., Schiff, L. B. and Baganoff, D., "Numerical Simulation of Unsteady, Viscous, High-Angle-of-Attack Flows Using a Partially Flux-split Algorithm," AIAA Paper No. 86-2179, Aug. 18-20, 1986.
- ¹⁸ Eggers, T., Sobieczky, H., and Center, K. B., "Design of Advanced Waveriders with High Aerodynamic Efficiency," AIAA Paper No. 93-5141, 1993.
- ¹⁹ Takashima, N. and Lewis, M. J., "Optimized Mission-Oriented Waverider Vehicle with base Closure," AIAA Paper No. 96-0810, Jan. 1996.
- ²⁰ Miller, R. W., Argow, B. M., Center, K. B., Brauckmann, G. J. and Rhode, M. N., "Experimental Verification of the Osculating Cones Method for Two Waverider Forebodies at Mach 4 and 6," AIAA Paper No. 98-0682, Jan. 12-15, 1998.
- ²¹ Graves, R. E. and Argow, B. M., "Aerodynamic Performance of an Osculating-Cones Waverider at High Altitudes," AIAA Paper No. 2001-2960, June, 2001.